


## Optical Radio-Frequency Phase Measurement With an Internal-State Rydberg Atom Interferometer

D.A. Anderson<sup>1</sup>,\* R.E. Sapiro<sup>1</sup>, L.F. Gonçalves<sup>1</sup>, R. Cardman<sup>1</sup>, and G. Raithel<sup>1</sup>  
*Rydberg Technologies Inc., Ann Arbor, Michigan 48103, USA*

 (Received 25 January 2021; revised 31 October 2021; accepted 8 March 2022; published 11 April 2022)

We realize and model an internal-state Rydberg atom interferometer for measurement of phase and intensity of radio-frequency (rf) electromagnetic waves. A phase reference is supplied to the atoms via a modulated laser beam, enabling atomic measurement of the rf wave's phase without a rf reference wave. The rf and optical fields give rise to closed interferometric loops within the atoms' internal Hilbert space. In our experiment, we construct interferometric loops in the state space  $\{6P_{3/2}, 90S_{1/2}, 91S_{1/2}, 90P_{3/2}\}$  of cesium and employ them to measure phase and intensity of a 5-GHz rf wave in a room-temperature vapor cell. Electromagnetically induced transparency on the  $6S_{1/2}$  to  $6P_{3/2}$  transition serves as an all-optical interferometer probe. The rf phase is measured over a range of  $\pi$ , and a sensitivity of 2 mrad is achieved. Measurements of rf phase and amplitude at submillimeter optical spatial resolution are demonstrated.

DOI: [10.1103/PhysRevApplied.17.044020](https://doi.org/10.1103/PhysRevApplied.17.044020)

Interferometry has been foundational to the advancement of science and technology since its inception at the end of the 19th century [1]. As a means to detect the phase of electromagnetic waves, interferometry is ubiquitous across disciplines from optics [2] and metrology [3] to cosmology [4,5], biomedical imaging [6], and optical [7] and radio-frequency (rf) [8] communications. Wave-particle duality [9] and interferometry [10] are fundamentally important for quantum mechanics, atomic and molecular physics, and precision metrology [11], from atom interferometry [12,13] and establishing fundamental principles of quantum measurement [14] to the emergence of quantum technologies [15] including atomic clocks [16,17] and inertial sensors [18] for precision timing and navigation.

Interferometric phase sensing is often performed by linear superposition of electromagnetic signal and reference waves of the same or similar frequencies, and using respective homodyne or heterodyne detectors. Multispectral phase sensing of fields that spread across the electromagnetic spectrum, from static fields to optical frequencies, can be accomplished by wave mixing in macroscopic nonlinear devices, such as nonlinear crystals, mixers, modulators, and demodulators. At a fundamental level, phase-coherent, nonlinear wave mixing also occurs in an individual atom, whose Hilbert space provides a grid of states that can be connected via electromagnetic couplings ranging from DC to optical and beyond. In this work, we present an atom interferometer for rf electromagnetic

waves: an interferometer in which optical fields and a single rf signal wave connect a pair of atomic states via two paths. The atom rf interferometer is employed for optical measurement of phase and intensity of a rf signal wave via readout of atomic populations [19,20].

In our atom rf interferometer, rf phase-reference information is transmitted to the atoms via a rf-modulated optical carrier field, preparing the atomic medium in a coherent superposition state of matter that is sensitive to phase and intensity of an incident signal rf wave. The interferometer is implemented with Rydberg states of atoms [21,22], which are highly susceptible to electric fields ranging from DC to terahertz. As a readout for the interferometer we use Rydberg electromagnetically induced transparency (EIT) [23], a method suitable for atom-based sensing in room-temperature vapors. We employ the atom rf interferometer to optically receive and measure the phase and intensity of a rf signal wave.

Radio-frequency sensing with Rydberg atoms employing fiducial rf reference waves to achieve phase-sensitive and reference-field-enhanced rf sensing has been previously demonstrated [19,20,24,25]. In these and related works [24,26–35], the atoms sense the intensity of a rf wave that consists of one or a superposition of multiple free-space rf fields. In the latter case, measurement of differential rf phases and heterodyne gain are afforded by the electromagnetic superposition principle for the rf fields [24,25] and coherent atomic dynamics do not play a key role. In another approach, in Ref. [32] it is proposed to attain phase sensitivity by interference of several Rydberg transitions coherently driven by four microwave fields. In the present experimental and theoretical study, we prepare

\*dave@rydbergtechnologies.com

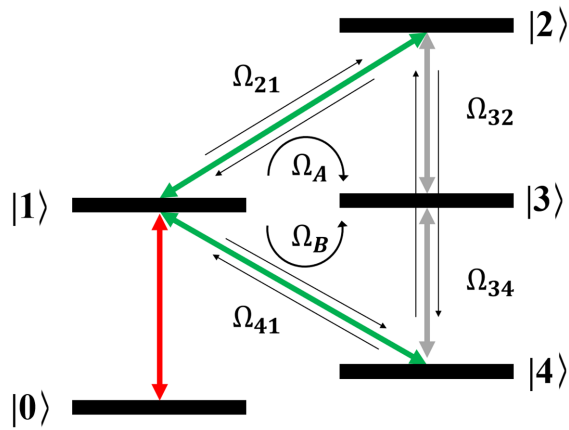


FIG. 1. Atom radio-frequency interferometer. Atomic states  $|2\rangle$  and  $|3\rangle$  and states  $|3\rangle$  and  $|4\rangle$  are electric dipole coupled by the same rf field (gray arrows); atomic states  $|1\rangle$  and  $|2\rangle$  and states  $|1\rangle$  and  $|4\rangle$  are coupled by two distinct optical fields (green arrows). All fields are phase coherent. The interferometric pathways, indicated by the thin circular arrows, are closed within the quantum state space. An additional optical field resonant with the  $|0\rangle$  to  $|1\rangle$  transition (red arrow) provides an optical readout for the interferometer.

and employ a coherent atomic medium that is sensitive to both phase and intensity of a rf signal wave, without requiring any additional rf reference wave.

The atomic energy-level and coupling scheme [19,20] is illustrated in Fig. 1. There,  $|0\rangle \rightarrow |1\rangle$  is an optical transition to probe the quantum interference. The  $|1\rangle \rightarrow |2\rangle$  and  $|1\rangle \rightarrow |4\rangle$  transitions are driven by optical fields (respective frequencies  $\omega_{21}$  and  $\omega_{41}$ ), and the  $|2\rangle \rightarrow |3\rangle$  and  $|4\rangle \rightarrow |3\rangle$  transitions by the signal rf field (frequency  $\omega_{\text{rf}}$ ). The frequency difference between the optical fields,  $\omega_{41} - \omega_{21}$ , equals  $2\omega_{\text{rf}}$ . In this way, a closed pair of interfering pathways from  $|1\rangle$  to  $|3\rangle$  is established, labeled *A* and *B* in

Fig. 1, with each path involving one optical and one rf photon. The respective transition amplitudes are

$$\begin{aligned}\Omega_A &= \frac{\Omega_{21} \Omega_{32}}{2\Delta_A} \exp[i(\phi_{\text{opt}} - \phi_{\text{rf}})], \\ \Omega_B &= \frac{\Omega_{41} \Omega_{34}}{2\Delta_B} \exp[i(-\phi_{\text{opt}} + \phi_{\text{rf}})],\end{aligned}\quad (1)$$

where  $\Omega_{nm}$  are (real-valued) magnitudes of the Rabi frequencies of the transitions from  $|m\rangle$  to  $|n\rangle$ , and  $\Delta_A$  and  $\Delta_B$  are detunings that occur in the respective paths, as specified below. The rf signal field carries a phase  $\phi_{\text{rf}}$ , and the pair of optical fields carries phases  $\pm\phi_{\text{opt}}$ .

The closed interferometric loop exhibits quantum interference between the two pathways associated with  $\Omega_A$  and  $\Omega_B$  (see Fig. 1). In the case studied, we may set  $|\Omega_A| = |\Omega_B| = \Omega_0$ . Phases accumulated along the optical beam paths are comprehensively accounted for by an optical phase difference  $2\phi_{\text{opt}}$ . The interferometric sum of the excitation amplitudes from  $|1\rangle$  to  $|3\rangle$  exhibits the following atom-interferometric phase dependence:

$$\Omega = 2\Omega_0 \cos(\phi_{\text{rf}} - \phi_{\text{opt}}). \quad (2)$$

Figures 2(a) and 2(b) show two implementations of the interferometric principle using Rydberg EIT [23] in a cesium room-temperature vapor cell. The 852-nm EIT probe laser is resonant on the  $|0\rangle = |6S_{1/2}(F=4)\rangle \rightarrow |1\rangle = |6P_{3/2}(F=5)\rangle$  transition (Rabi frequency  $\Omega_P = \Omega_{10}$ ), and two 510-nm EIT coupler-laser modes simultaneously drive the  $|1\rangle \rightarrow |4\rangle = |90S\rangle$  and  $|1\rangle \rightarrow |2\rangle = |91S\rangle$  Rydberg transitions (respective Rabi frequencies  $\Omega_{C^-} = \Omega_{41}$  and  $\Omega_{C^+} = \Omega_{21}$ ). The Rydberg states  $|4\rangle$  and  $|2\rangle$  are near-resonantly coupled by the (same) rf field to Rydberg state  $|3\rangle = |90P_{3/2}\rangle$ , with respective Rabi frequencies  $\Omega_{34} \approx \Omega_{32} =: \Omega_{\text{rf}}$ .

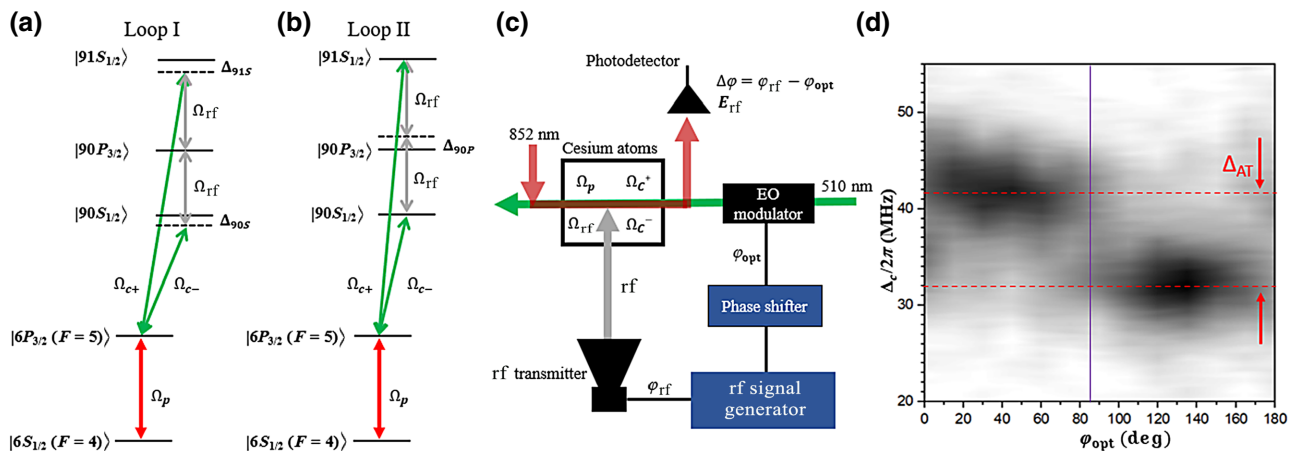


FIG. 2. Energy-level diagrams for interferometric loops (a) I and (b) II in a cesium vapor with Rydberg EIT. (c) Experimental setup. (d) Phase measurement of a 5.092-GHz electromagnetic field using interferometric loop II.

In interferometric loop I, shown in Fig. 2(a), the pair of two-photon couplings  $|1\rangle \rightarrow |3\rangle$  are both exactly two-photon resonant, with two-photon Rabi frequencies  $\Omega_A$  and  $\Omega_B$  as defined in Eq. (1). The intermediate detunings from levels  $|4\rangle$  and  $|2\rangle$ , labeled  $\Delta_{90S}$  and  $\Delta_{91S}$  in Fig. 2(a), are generally different but typically have similar magnitude. This system exhibits interference and phase sensitivity as exhibited in Eqs. (1) and (2).

In interferometric loop II, shown in Fig. 2(b), the optical couplings  $|1\rangle \rightarrow |2\rangle$  and  $|1\rangle \rightarrow |4\rangle$  are both essentially on-resonance. The rf field couples levels  $|4\rangle$  and  $|2\rangle$  in second order via level  $|3\rangle$ , with intermediate-state detuning denoted  $\Delta_{90P}$ . The detuning from two-photon resonance,  $\Delta_{\text{rf}} = 2\omega_{\text{rf}} - (W_2 - W_4)/\hbar$  with level energies  $W_i$ , is typically held near zero, except in Fig. 4(b) where we explore the effects of a nonzero  $\Delta_{\text{rf}}$ . The interference in loop II is seen by first noting that the two-photon rf coupling generates a pair of Autler-Townes (AT)-split states, with AT splitting  $\Delta_{\text{AT}}$ , that are orthogonal superpositions of  $|2\rangle$  and  $|4\rangle$ . These states are excited by the two optical coupler-laser modes with Rabi frequencies  $\Omega_{C\pm}$ . The quantum coherence of the bare atomic constituents  $|2\rangle$  and  $|4\rangle$  within the AT states, and the phase coherence of the two optical excitation paths with each other and with the rf field impinging onto the atoms, lead to an interferometric dependence of the net excitation amplitude on  $\phi_{\text{opt}} - \phi_{\text{rf}}$ . The signal in loop II, observed as a function of the (unmodulated) coupler-laser detuning  $\Delta_C$  and  $\phi_{\text{opt}}$ , consists of two bands that are separated in  $\Delta_C$  by a two-photon AT splitting  $\Delta_{\text{AT}}$  [see Fig. 2(d)]. Due to the orthogonality of the AT states, the EIT signals on the AT pair of loop-II bands have orthogonal dependencies on the phase  $\phi_{\text{opt}}$ .

The EIT probe transmission signal is related to the coupler-light-induced coupling strength  $|\Omega|^2$ , with  $\Omega$  in the form of Eq. (2). Both loops I and II allow measurement of an unknown  $\phi_{\text{rf}}$  via tuning of  $\phi_{\text{opt}}$ , or vice versa. Loop II further yields the rf field intensity by measuring the two-photon AT splitting  $\Delta_{\text{AT}}$  and the detuning  $\Delta_{90P}$ . In the case  $\Delta_{\text{rf}} = 0$ , the rf intensity,  $I_{\text{rf}} = (1/2)c\epsilon_0 E_{\text{rf}}^2$  with rf electric field  $E_{\text{rf}}$ , follows from  $\Delta_{\text{AT}} = \Omega_{34}\Omega_{32}/(2\hbar^2\Delta_{90P}) = d_{34}d_{32}E_{\text{rf}}^2/(2\hbar^2\Delta_{90P})$ , with transition electric dipole matrix elements  $d_{nm}$ .

Our experimental setup, illustrated in Fig. 2(c), utilizes probe (852 nm) and coupler (510 nm) laser sources that are frequency stabilized to approximately 100 kHz. The 510-nm coupler laser beam is passed through an electro-optic phase modulator (PM) that is modulated at the rf frequency  $\omega_{\text{rf}} \approx 5$  GHz. The first-order PM sidebands provide a pair of coupler modes separated by  $2\omega_{\text{rf}}$  in frequency. The EIT coupler modes co-propagate and are counter-aligned with the EIT probe. The optical phase shift  $\phi_{\text{opt}}$  is implemented by phase shifting the rf supplied by the signal generator to the PM. The optical field modes generating the couplings  $\Omega_{C\pm}$  transmit the phase  $\phi_{\text{opt}}$  to the atoms, with opposite sign [see Eq. (1)]. The signal generator also feeds a horn

antenna that transmits the 5-GHz free-space signal wave to the cesium atoms, which are located in the far field of the antenna. The EIT probe transmission signal is collected on a photoreceiver for read out of the rf interferometer while the frequency offset of the coupler-laser source,  $\Delta_C$ , is scanned. In the measurements, we map the EIT probe transmission,  $T$ , in the  $(\Delta_C, \phi_{\text{opt}})$  plane, revealing the rf phase  $\phi_{\text{rf}}$  (loops I and II) and intensity (loop II).

In Fig. 2(d) we determine a fixed, unknown phase  $\phi_{\text{rf}}$  using loop II by measuring  $T(\Delta_C, \phi_{\text{opt}})$  for  $\omega_{\text{rf}} = 2\pi \times 5.092$  GHz, a case that is near two-photon rf resonance  $\Delta_{\text{rf}} \sim 0$  for the Rydberg states chosen in this work. Two EIT bands, corresponding to AT-split states separated by  $\Delta_{\text{AT}} \approx 2\pi \times 10$  MHz in  $\Delta_C$ , extend along the  $\phi_{\text{opt}}$  direction and are modulated in  $\phi_{\text{opt}}$  with a period of  $\pi$ , as generally expected by taking the square of Eq. (2). The two EIT bands of loop II are shifted in  $\phi_{\text{opt}}$  by  $\pi/2$  relative to each other due to the orthogonality of the two AT-split states. The fringe visibility well exceeds 50%, as seen more clearly in Fig. 3, with limiting factors discussed in our model below. We choose the inflection points of the loop-II signals to assign a value to the phase  $\phi_{\text{rf}}$  of the rf wave to be measured. In Fig. 2(d), the measured rf phase is  $\phi_{\text{rf}} = 85^\circ \pm 5^\circ$ .

In Fig. 3(a) we show a similar measurement of both loops I and II, and in Fig. 3(c) we plot individual EIT spectra  $T(\Delta_C)$  at  $\phi_{\text{opt}}$  values where the loop signals are extremal as a function of  $\phi_{\text{opt}}$ . There is a total of three EIT bands at certain values of  $\Delta_C$ , with the lowest-frequency band corresponding to loop I and the two higher-frequency ones

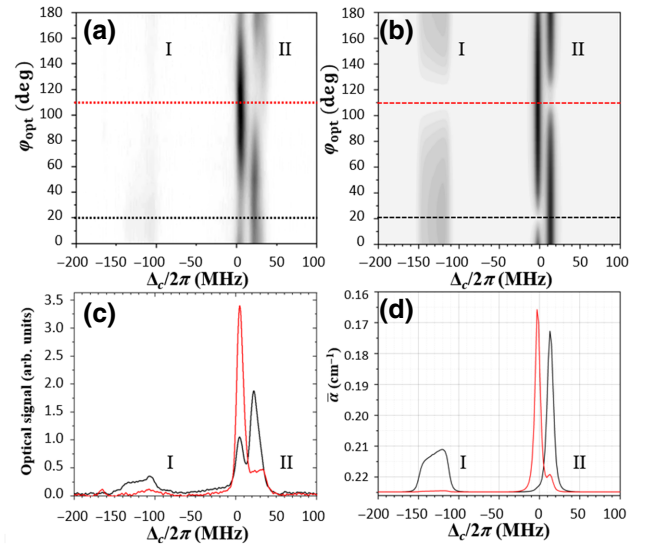


FIG. 3. (a) Measurement of  $T(\Delta_C, \phi_{\text{opt}})$  to find the phase of a 5.092-GHz free-space rf wave. Signals from loops I and II are labeled. (b) Calculation of cell probe absorption  $\tilde{\alpha}(\Delta_C, \phi_{\text{opt}})$  for conditions as in the experiment (a). Experimental (c) and calculated (d) EIT spectra  $T(\Delta_C)$  and  $\tilde{\alpha}(\Delta_C)$  at fixed values of  $\phi_{\text{opt}}$  indicated by dashed lines in (a) and (b), respectively.

to the two AT-split bands of loop II. Here,  $\Delta_{\text{AT}}/(2\pi) = 18 \pm 1$  MHz, and  $\Delta_{90P}/(2\pi) = -130 \pm 15$  MHz, taken to be the separation between the center of the loop-I band and the midpoint between the two loop-II bands. The loop-I signal is considerably weaker than that of loop II due to the presence of a weak DC electric field. The DC field shifts the loop-I signal from its zero-field value of  $\Delta_C/(2\pi) = -55$  MHz to approximately  $-130$  MHz, and broadens it over a range of about 30 MHz. Using the experimental values for  $\Delta_{\text{AT}}$  and  $\Delta_{90P}$  and calculated values of  $d_{34} = 3942 ea_0$  and  $d_{32} = 3849 ea_0$ , one finds  $E_{\text{rf}} = 1.4 \pm 0.2$  V/m.

To numerically model the atom rf interferometer measurements in Figs. 3(a) and 3(c), we obtain the steady-state density operator  $\hat{\rho}$  of the Lindblad equation for the five-level system of Fig. 2. The absorption coefficient of the cesium vapor for the probe beam is given by

$$\alpha = \frac{2\pi}{\lambda_P} \frac{2n_V d_{10}}{\epsilon_0 E_P} \int P(v) \text{Im}(\rho_{01}) dv. \quad (3)$$

Here,  $n_V$  is the density of cesium atoms in the  $F = 4$  ground state at 293 K,  $d_{10} = 1.9 ea_0$  is the probe electric dipole matrix element,  $\lambda_P$  is the probe-laser wavelength and  $E_P$  is its electric field amplitude, and  $P(v)$  is the normalized one-dimensional Maxwell velocity distribution at 293 K. The coherence  $\rho_{01}$  depends on Rabi frequencies, field phases, decay rates, atom-field detunings, and atom velocity  $v$ . The DC-field-free dressed Rydberg-level detunings at  $v = 0$  are  $\Delta_{90S} = 2\pi \times 55.1$  MHz  $- \Delta_C$ ,  $\Delta_{90P} = -\Delta_C$ , and  $\Delta_{91S} = 2\pi \times 55.1$  MHz  $- \Delta_C$ . We use an optical EIT probe Rabi frequency at the beam center of  $\Omega_{10} = 2\pi \times 7.7$  MHz, and EIT coupler Rabi frequencies at the beam center of  $\Omega_{21} \approx \Omega_{41} = 2\pi \times 1.0$  MHz. In Figs. 3(a) and 3(c) the measured rf Rabi frequencies are  $\Omega_{34} = 64$  MHz and  $\Omega_{23} = 62$  MHz.

We calculate weighted averages of  $\alpha$  from Eq. (3) over the transverse Gaussian profile of the laser beams and over distributions of the DC electric field,  $P_E(E)$ , which leads to the shift and broadening of the loop-I signal in Figs. 3(a) and 3(c). Here, the measured results are reproduced by a flat distribution  $P_E(E)$  ranging from  $E = 29$  to 41 mV/cm. Figures 3(b) and 3(d) show the calculated averaged absorption coefficient,  $\bar{\alpha}(\Delta_C, \phi_{\text{opt}})$ , and respective cuts at selected phases,  $\phi_{\text{opt}}$ , for conditions as in Figs. 3(a) and 3(c). Good agreement is found between experiment and calculation, reproducing the relative phases, AT splittings, and linewidths of the signal bands.

The higher-frequency loop-II band in the experimental data  $T(\Delta_C, \phi_{\text{opt}})$  exhibits a correlation between the phase of the EIT signal and the detuning  $\Delta_C$ . This is attributed to a spatial correlation between the DC field and the optical-beam propagation phase  $\Delta k x$ , with  $\Delta k$  denoting the wave number difference between the two coupler modes and  $x$  for the position along the coupler-beam direction. The reduced

visibility in the phase dependencies of the loop-I and loop-II signals in Fig. 3(c) relative to those in Fig. 3(d) is attributed to the propagation phase  $\Delta k x$ .

In Fig. 4(a) we verify the dependence of the loop-II splitting,  $\Delta_{\text{AT}}$ , on  $E_{\text{rf}}$  for the case of two-photon rf resonance,  $\Delta_{\text{rf}} \approx 0$ . In that case, one expects  $\Delta_{\text{AT}} \propto E_{\text{rf}}^2$ , in good qualitative agreement with the measurements shown in Fig. 4(a). For nonzero  $\Delta_{\text{rf}}$ , the loop-II splitting is given by  $\sqrt{\Delta_{\text{AT}}^2 + \Delta_{\text{rf}}^2}$ , the effective off-resonant two-photon Rabi frequency. This behavior is evident in Fig. 4(b), where  $\Delta_{\text{rf}} \approx 10$  MHz in the left-hand panel and  $\Delta_{\text{rf}} \approx 0$  in the right-hand panel. The visibility of the phase-dependent modulation of the loop-I and loop-II bands is expected to diminish with increasing  $|\Delta_{\text{rf}}|$ , which is supported by the measurements in Fig. 4(b). The measurements in Figs. 4(a) and 4(b) agree well with simulations (not shown).

The static rf phase resolution in the phase measurements in Figs. 2 and 3 is about  $5^\circ$ . In the last component of the present work, we determine the phase resolution achievable using a dynamic interferometric method. For a fixed

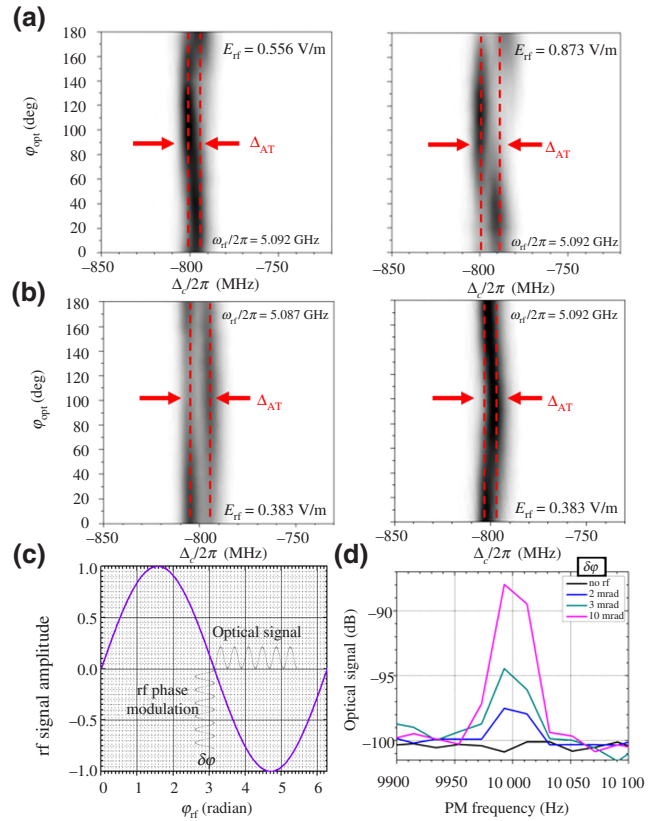


FIG. 4. (a) Loop-II signal for the indicated rf electric fields,  $E_{\text{rf}}$ , for on-resonant two-photon rf transition ( $\Delta_{\text{rf}} \approx 0$ ). (b) Loop-II signal for two-photon detuning  $\Delta_{\text{rf}} \approx 0$  (right panel) and  $\Delta_{\text{rf}} \approx 10$  MHz (left panel), for fixed and small  $E_{\text{rf}}$ . (c) Mapping of PM,  $\delta\phi$ , into a modulated EIT signal,  $\delta V$ . (d) Measured power spectrum of the EIT signal,  $\delta V$ , for the indicated values of  $\delta\phi$  for a PM frequency of 10 kHz.

optical phase near the inflection point  $\frac{\partial^2}{\partial \phi_{\text{opt}}^2} T(\Delta_{C0}, \phi_{\text{opt}}) = 0$ , with  $\Delta_{C0}$  set at a loop II-band, we apply a weak PM of known amplitude  $\delta\phi_{\text{rf}}$  to the rf field, with a PM frequency of 10 kHz. Since variations of optical and rf phases have equivalent effects on the optical signal  $T$ , lock-in detection of  $T$  at the PM frequency yields a modulation amplitude  $\delta T = \left[ \frac{\partial}{\partial \phi_{\text{opt}}} T(\Delta_{C0}, \phi_{\text{opt}}) \right] \delta\phi_{\text{rf}}$ . In Figs. 4(c) and 4(d) we observe a minimum detectable  $\delta\phi_{\text{rf}} \approx 0.1^\circ = 2$  mrad, limited by the rf hardware.

In summary, we realize an atom rf interferometer, employ it for all-optical phase measurement of a rf wave with a cesium vapor sensor, and develop a quantum model that reproduces all observed features. A phase resolution of 2 mrad is achieved and rf phase and field measurements traceable to the International System of Units (SI) for SI-traceability are demonstrated at submillimeter optical spatial resolution. Atom rf interferometry provides a platform enabling capabilities in optical and rf phase, frequency, and amplitude signal reception, measurement, and imaging, relevant to a broad range of applications in rf and communications technology.

### ACKNOWLEDGMENTS

This work is supported by Rydberg Technologies Inc.

- 
- [1] Albert A. Michelson, On the Relative Motion of the Earth and of the Luminiferous Ether, *Am. J. Sci.* **22**, 120 (1881).
- [2] Max Born, Emil Wolf, A. B. Bhatia, P. C. Clemmow, D. Gabor, A. R. Stokes, A. M. Taylor, P. A. Wayman, W. L. Wilcock, *Principles of Optics: Electromagnetic Theory of Propagation, Interference and Diffraction of Light* (Cambridge University Press, Cambridge, 1999).
- [3] R. K. Chang, J. Ducuing, and N. Bloembergen, Relative Phase Measurement Between Fundamental and Second-Harmonic Light, *Phys. Rev. Lett.* **15**, 6 (1965).
- [4] Rafal Demkowicz-Dobrzański, Marcin Jarzyna, and Jan Kołodyński, *Chapter Four - Quantum Limits in Optical Interferometry*, edited by E. Wolf, *Progress in Optics*, Vol. 60 (Elsevier, 2015), p. 345.
- [5] L. G. Spitler *et al.*, A repeating fast radio burst, *Nature* **531**, 202 (2016).
- [6] C. Depeursinge, G. Popescu, and Y. Park, Quantitative phase imaging in biomedicine, *Nat. Photon* **12**, 578 (2018).
- [7] R. M. Gagliardi, and S. Karp, *Optical Communications* (Wiley Interscience, New York, NY, 1976).
- [8] J. A. Flemming, *The Principles of Electric Wave Telegraphy and Telephony* (Longmans, Green, 1919).
- [9] Louis De Broglie, Ph.D. thesis, Migration-université en cours d'affectation, 1924.
- [10] Norman F. Ramsey, A molecular beam resonance method with separated oscillating fields, *Phys. Rev.* **78**, 695 (1950).
- [11] Alexander D. Cronin, Jörg Schmiedmayer, and David E. Pritchard, Optics and interferometry with atoms and molecules, *Rev. Mod. Phys.* **81**, 1051 (2009).
- [12] David W. Keith, Christopher R. Ekstrom, Quentin A. Turchette, and David E. Pritchard, An Interferometer for Atoms, *Phys. Rev. Lett.* **66**, 2693 (1991).
- [13] Mark Kasevich, and Steven Chu, Atomic Interferometry Using Stimulated Raman Transitions, *Phys. Rev. Lett.* **67**, 181 (1991).
- [14] M. Brune, E. Hagley, J. Dreyer, X. Maître, A. Maali, C. Wunderlich, J. M. Raimond, and S. Haroche, Observing the Progressive Decoherence of the “Meter” in a Quantum Measurement, *Phys. Rev. Lett.* **77**, 4887 (1996).
- [15] A. G. J. MacFarlane, Jonathan P. Dowling, and Gerard J. Milburn, Quantum technology: the second quantum revolution, *Philos. Trans. R. Soc. London. Ser. A: Math. Phys. Eng. Sci.* **361**, 1655 (2003).
- [16] L. Essen, and J. V. L. Parry, An atomic standard of frequency and time interval: A caesium resonator, *Nature* **176**, 280 (1955).
- [17] Andrew D. Ludlow, Martin M. Boyd, Jun Ye, E. Peik, and P. O. Schmidt, Optical atomic clocks, *Rev. Mod. Phys.* **87**, 637 (2015).
- [18] Ying-Ju Wang, Dana Z. Anderson, Victor M. Bright, Eric A. Cornell, Quentin Diot, Tetsuo Kishimoto, Mara Prentiss, R. A. Saravanan, Stephen R. Segal, and Saijun Wu, Atom Michelson Interferometer on a Chip Using a Bose-Einstein Condensate, *Phys. Rev. Lett.* **94**, 090405 (2005).
- [19] D. A. Anderson, G. Raithel, E. G. Paradis, and R. E. Sapiro, Atom-based electromagnetic field sensing element and measurement system, Patent US20190187198A1 (2018).
- [20] D. A. Anderson, R. E. Sapiro, and G. Raithel, Rydberg atoms for radio-frequency communications and sensing: Atomic receivers for pulsed rf field and phase detection, *IEEE Aerosp. Electron. Syst. Mag.* **35**, 48 (2020).
- [21] H. A. Bethe, and E. E. Salpeter, *Quantum Mechanics of One- and Two-Electron Atoms* (Springer, Berlin, 1957).
- [22] T. F. Gallagher, *Rydberg Atoms* (Cambridge University Press, Cambridge, 1994).
- [23] A. K. Mohapatra, T. R. Jackson, and C. S. Adams, Coherent Optical Detection of Highly Excited Rydberg States Using Electromagnetically Induced Transparency, *Phys. Rev. Lett.* **98**, 113003 (2007).
- [24] Matthew T. Simons, Abdulaziz H. Haddab, Joshua A. Gordon, and Christopher L. Holloway, A rydberg atom-based mixer: Measuring the phase of a radio frequency wave, *Appl. Phys. Lett.* **114**, 114101 (2019).
- [25] Mingyong Jing, Ying Hu, Jie Ma, Hao Zhang, Linjie Zhang, Liantuan Xiao, and Suotang Jia, Atomic superheterodyne receiver based on microwave-dressed rydberg spectroscopy, *Nat. Phys.* **16**, 911 (2020).
- [26] Jonathon A. Sedlacek, Arne Schwettmann, Harald Kübler, Robert Löw, Tilman Pfau, and James P. Shaffer, Microwave electrometry with rydberg atoms in a vapour cell using bright atomic resonances, *Nat. Phys.* **8**, 819 (2012).
- [27] Christopher L. Holloway, Joshua A. Gordon, Andrew Schwarzkopf, David A. Anderson, Stephanie A. Miller, Nithiwadee Thaicharoen, and Georg Raithel, Sub-wavelength imaging and field mapping via electromagnetically induced transparency and autler-townes splitting in rydberg atoms, *Appl. Phys. Lett.* **104**, 244102 (2014).
- [28] D. A. Anderson, A. Schwarzkopf, S. A. Miller, N. Thaicharoen, G. Raithel, J. A. Gordon, and C. L. Holloway,

- Two-photon microwave transitions and strong-field effects in a room-temperature rydberg-atom gas, *Phys. Rev. A* **90**, 043419 (2014).
- [29] D. A. Anderson, S. A. Miller, G. Raithel, J. A. Gordon, M. L. Butler, and C. L. Holloway, Optical Measurements of Strong Microwave Fields with Rydberg Atoms in a Vapor Cell, *Phys. Rev. Appl.* **5**, 034003 (2016).
- [30] D. A. Anderson, G. Raithel, N. Thaicharoen, S. A. Miller, and A. Schwarzkopf, Atom-based electromagnetic radiation electric-field and power sensor, Patent US 9, 970, 973 B2 (2017).
- [31] D. A. Anderson, G. Raithel, M. Simons, and C. L. Holloway, Quantum-optical spectroscopy for plasma electric field measurements and diagnostics, [arXiv:1712.08717](https://arxiv.org/abs/1712.08717) (2017).
- [32] D. Shylla, E. O. Nyakang'o, and K. Pandey, Highly sensitive atomic based MW interferometry, *Sci. Rep.* **8**, 8692 (2018).
- [33] David Alexander Anderson, Rachel Elizabeth Sapiro, and Georg Raithel, An atomic receiver for am and fm radio communication, *IEEE Trans. Antennas Propag.* **69**, 2455 (2021).
- [34] David H. Meyer, Kevin C. Cox, Fredrik K. Fatemi, and Paul D. Kunz, Digital communication with rydberg atoms and amplitude-modulated microwave fields, *Appl. Phys. Lett.* **112**, 211108 (2018).
- [35] David H. Meyer, Zachary A. Castillo, Kevin C. Cox, and Paul D. Kunz, Assessment of rydberg atoms for wideband electric field sensing, *J. Phys. B: At. Mol. Opt. Phys.* **53**, 034001 (2020).